AIAA JOURNAL
Vol. 48, No. 11, November 2010

Klebanoff-Mode Modeling and Bypass-Transition Prediction

O. Vermeersch* and D. Arnal†
ONERA, 31055 Toulouse Cedex 4, France

DOI: 10.2514/1.J050002

A number of experiments have demonstrated that the classical Tollmien–Schlichting transitional mechanism is no longer valid inside boundary layers subjected to intense external disturbances. In such a case, perturbations in the laminar region take the form of three-dimensional streamwise-elongated structures, the Klebanoff modes, also called streaks, which may be strongly amplified, resulting in an early bypass transition. This amplification is described by the transient-growth theory. In the present paper, a semi-empirical model has been developed for the prediction of this type of bypass transition. It is based on the resolution of two parabolic linear transport equations for the longitudinal velocity and the temperature fluctuations. A transition criterion is then formed based on the ratio of streak production and dissipation. Several sets of experimental data were used for validation of the proposal model, assessing the effects of pressure gradients and of freestream turbulence properties.

Nomenclature

$\langle A \rangle$	=	average
$\tilde{A}$	=	density weighted average, $\langle \rho A \rangle / \langle \rho \rangle$
A_{st}	=	constant used to fix the streaks amplitude
a'	=	fluctuation
C	=	constant fixing the bypass-transition threshold
C_f	=	skin-friction coefficient
cc	=	complex conjugate
C_p	=	specific heat constant for constant pressure process
$G(y)$	=	dimensionless wall-normal velocity perturbation inside the boundary layer
H	=	shape factor
h	=	enthalpy
h_i	=	total enthalpy
L	=	streamwise scale
L_e	=	dissipative turbulence length scale
M	=	Mach number
$\max_{\forall y}(\cdot)$	=	maximum in the boundary-layer thickness
$\tilde{P}$, π'	=	pressure
Pr	=	Prandtl number
Re_L	=	Reynolds number relative to L
Re_θ	=	Reynolds number based on the momentum thickness
$\tilde{T}$, θ'	=	temperature
Tu	=	freestream turbulent level
t	=	time
$\tilde{U}$, u'	=	streamwise velocity
$\tilde{V}$, v'	=	normal velocity
$\tilde{W}$, w'	=	spanwise velocity
x	=	streamwise coordinate
y	=	wall-normal coordinate
z	=	spanwise coordinate
β	=	spanwise wave number
γ	=	intermittency function
δ	=	wall-normal scale, $L/\sqrt{Re_L}$
δ_1	=	displacement thickness
δ_{99}	=	boundary-layer thickness
θ	=	momentum thickness
κ	=	conductivity
μ	=	dynamic viscosity
ρ	=	density
ω	=	frequency, $2\pi f$

Subscripts

e	=	boundary-layer outer-edge value
exp	=	experimental value
num	=	numerical value
st	=	relative to streak
T	=	value at the transition location
t	=	relative to turbulence
0	=	leading-edge value
∞	=	freestream value

Presented as Paper 2009-3807 at the 27th AIAA Applied Aerodynamics Conference, San Antonio, TX, 22–25 June 2009; received 16 June 2009; revision received 15 February 2010; accepted for publication 11 August 2010.

*Research Engineer, Department of Modelling Aerodynamics and Energetics, Transition and Instability Group, 2 Avenue Edouard Belin, B.P. 4025.

†Head of Research Unit, Department of Modelling Aerodynamics and Energetics, Transition and Instability Group, 2 Avenue Edouard Belin, B.P. 4025.

I. Introduction

ALTHOUGH the flow inside turbomachines is strongly perturbed, strong accelerations may force relaminarization on the blades, and the laminar–turbulent transition and its location may have a significant impact on turbine efficiency. More generally, laminar–turbulent transition is known to correspond to an increase in heat transfer and in the drag coefficient. In the case of turbine blades, transition prediction is a challenging task because of the high freestream turbulence (FST) resulting from the rotor wake and because of strong pressure gradients. In such types of flows, it has been shown using flow visualizations [1] and hot-wire measurements [2] that boundary-layer disturbances called Klebanoff modes become the dominant instabilities. They were named in recognition of Klebanoff's experimental contribution [3].

A systematic study of the effect of freestream turbulence was conducted in 1978 by Arnal and Juillen [4], with turbulence levels between 0.12 and 1.2%, generated by turbulence grids. Whereas classical Tollmien–Schlichting (TS) were observed at the lowest turbulence level, disturbances of a different nature were observed at $Tu = 1.2\%$. The largest disturbances were then characterized by frequency modes lower than those of TS instabilities and amplitudes reaching as much as 10% of the external velocity just upstream of the transition onset.

In 1985, Kendall [5] observed streamwise-elongated structures with narrow spanwise scales inside a boundary layer submitted to external grid turbulence. He denoted these disturbances as Klebanoff modes and measured that their amplitudes were amplified in $\sqrt{x}$ (i.e., proportional to the boundary-layer thickness).

Many other experiments concerning boundary layers subjected to significant freestream turbulence level have demonstrated that laminar–turbulent transition may occur at Reynolds numbers lower than those predicted by the classical linear theory. It was first proposed to look at the nonlinear terms of Navier–Stokes equations, but according to Henningson [6], these nonlinear terms just share energy among eigenmodes. Another process was to be identified; it is now agreed that transient growth may result from the interaction of nonnormal eigenfunctions [7,8]. The first multimode analysis was performed by Ellingsen and Palm [9]; they established that a vertical velocity fluctuation in a shear flow can bring about the emergence of longitudinal velocity fluctuations. This phenomenon was called *lift-up effect* by Landahl [10]. A longitudinal vortex superimposed to the boundary-layer shear pushes up low-speed particles from the wall to the top of the shear layer and pulls down high-speed particles toward the wall, leading to a spanwise alternation of backward and forward streaky structures called Klebanoff modes.

If the energy of the Klebanoff modes raises above a given limit, an early laminar–turbulent transition can be triggered: this is the so-called bypass transition, meaning that the usual transition, driven by the TS waves, does not occur. Therefore, in certain circumstances, restricting the study of stability to the most amplified mode (TS wave) is not sufficient.

The growth mechanism of streaks was identified theoretically as a result of transient amplification of perturbations (see, for instance, Andersson et al. [11] and Luchini [12]). They employed an optimal technique based on the resolution of the linear stability equation system of the boundary layer and its corresponding adjoint formulation. They found that streamwise vortices at the inlet of a spatially developing boundary layer transformed downstream into streaks of spanwise alternating high and low streamwise velocity. The amplitude of these resulting disturbances was shown to grow as $\sqrt{x}$, as measured by Kendall [5] more than 10 years earlier.

Tumin and Reshotko [13] and Zuccher et al. [14] add an equation for the temperature fluctuation to study transient growth of compressible boundary layers; the initial optimal perturbations correspond to longitudinal vortices and lead to the formation of streamwise streaks in the boundary layer. They pointed out that at low Mach number ($M = 0.5$), wall cooling considerably increases the amplification of the streaks.

One of the most important points concerns the receptivity mechanism of the boundary layer to high-intensity external disturbances: i.e., how these external perturbations lead to the formation of longitudinal streaks in the laminar part of the boundary layer. Measurements have demonstrated that the boundary-layer response to freestream turbulence is streaky structures. The key event is the receptivity process: i.e., the link between perturbations outside and inside the boundary layer. This process is very difficult to analyze, because it depends on many parameters, such as intensity, scale, isotropy, and power spectral density of the freestream turbulence. From an experimental viewpoint, studying receptivity is very intricate because of the random character of the introduced disturbances, which are usually generated by a grid.

Jonàš et al. [15] have shown experimentally that the transition position was influenced by the dissipation length scale of the freestream turbulence. This important result is confirmed by the direct numerical simulations (DNS) of Brandt et al. [16]. A possible explanation lies in the shear sheltering effect, which describes the protection of the boundary layer from the high frequencies by the shear stress; in the external flow, instabilities are convected without any pressure gradient, but at the border of the boundary layer, pressure perturbation does not vanish and creates a penetration instability mechanism inside the boundary layer, which results from a local competition between the external flow and the boundary layer. Several experimental results [2,17] as well as DNS [18] evidenced the filtering of the turbulence spectrum toward low frequencies inside the boundary layer. Hernon et al. [19] were able to measure the penetration depth, which describes this ability of a given external perturbation to penetrate the boundary layer. In the numerical results of Jacobs and Durbin [18], they found that when moving downstream, the penetration depth was decreasing: i.e., as the frequency increased, the boundary-layer sensitivity to external perturbations decreased.

The main objective of this paper is to present a new simplified semi-empirical model describing the dynamics of streaks. The model will be applied to predict transition for boundary layers subjected to high freestream turbulence.

II. Governing Equations

A. Base Flow Equations

If the FST level is too high, the influence of the streaks on the mean flow cannot be neglected in the laminar zone. Indeed, experiments have shown that streamwise velocity fluctuations can reach 10% of the external velocity before transition occurs. A natural approach consists of applying the boundary-layer turbulent equations to describe the laminar zone, even though the fully turbulent state has not been reached yet.

These equations are set in the general case of a compressible boundary layer using the density weighted average defined by relation (1). Total quantities are split into a mean part and a perturbation. In addition, correlations between speed and viscosity, temperature and conductivity fluctuations and triple correlations are supposed to be negligible:

$$A = \tilde{A} + a' \quad \text{such as } \tilde{A} = \frac{\langle \rho A \rangle}{\langle \rho \rangle}, \qquad \text{with } A = (\mathrm{U}, \mathrm{V}, \mathrm{W}, \mathrm{T}, \mathrm{h_i})$$
$$\left\langle \mu \frac{\mathrm{d}U_i}{\mathrm{d}x_j} \right\rangle = \langle \mu \rangle \cdot \left\langle \frac{\mathrm{d}U_i}{\mathrm{d}x_j} \right\rangle, \qquad \left\langle \kappa \frac{\mathrm{d}T}{\mathrm{d}x_j} \right\rangle = \langle \kappa \rangle \cdot \left\langle \frac{\mathrm{d}T}{\mathrm{d}x_j} \right\rangle$$
$$\langle \rho u_i' u_j' \rangle = \langle \rho \rangle \cdot \langle u_i' u_j' \rangle, \qquad \langle \rho u_j' \theta' \rangle = \langle \rho \rangle \cdot \langle u_j' \theta' \rangle \tag{1}$$

To make the equations dimensionless, typical length and velocity scales have been introduced. In the laminar region, fluctuations take the form of spanwise alternated low- and high-velocity streaky structures; as mentioned before, optimal disturbance numerical studies [11,12] have shown that these streaks are spatially amplified proportionally to $\sqrt{x}$. Therefore, a typical scale of geometry, L (for instance the length of the flat plate or the chord of the wing), is used to normalize the streamwise coordinate. In the wall-normal direction, a typical boundary-layer thickness $\delta = L/\sqrt{Re_L}$ is applied to characterize the diffusion process. The continuity equation, satisfied by the Klebanoff modes implies that if u'_{st} is on the order of U_0, then $v'_{\mathrm{st}} = \mathcal{O}(U_0/\sqrt{Re_L})$. These scales, introduced by Prandtl [20] to study laminar boundary layers, are summarized in Table 1. In the turbulent area, contrary to the laminar zone, u'_t and v'_t are of the same order of magnitude; therefore, streamwise derivatives are smaller than wall-normal derivatives and can thus be neglected.

These assumptions for a two-dimensional compressible boundary-layer flow lead to the following system of Reynolds-averaged Navier–Stokes equations that describes the flow for both laminar and turbulent states:

$$\frac{\partial}{\partial x}(\langle \rho \rangle \tilde{U}) + \frac{\partial}{\partial y}(\langle \rho \rangle \tilde{V}) = 0 \tag{2a}$$

$$\langle \rho \rangle \tilde{U} \frac{\partial \tilde{U}}{\partial x} + \langle \rho \rangle \tilde{V} \frac{\partial \tilde{U}}{\partial y} = \rho_e U_e \frac{\mathrm{d}U_e}{\mathrm{d}x} + \frac{\partial}{\partial y}\left(\langle \mu \rangle \frac{\partial \tilde{U}}{\partial y} \right) - \gamma \cdot \frac{\partial \langle \rho \rangle \langle u'v' \rangle_t}{\partial y} - (1-\gamma) \cdot \left(- \frac{\partial \langle \rho \rangle \langle u'u' \rangle_{\mathrm{st}}}{\partial x} - \frac{\partial \langle \rho \rangle \langle u'v' \rangle_{\mathrm{st}}}{\partial y} \right) \tag{2b}$$

$$\langle \rho \rangle \tilde{U} \frac{\partial \tilde{h}_i}{\partial x} + \langle \rho \rangle \tilde{V} \frac{\partial \tilde{h}_i}{\partial y} = \frac{\partial}{\partial y}\left(\langle \mu \rangle \tilde{U} \frac{\partial \tilde{U}}{\partial y} + \langle \kappa \rangle \frac{\partial \tilde{T}}{\partial y} \right) - \gamma \cdot \frac{\partial}{\partial y}(\langle \rho \rangle \tilde{U} \langle u'v' \rangle_t + \langle \rho \rangle \langle v'h' \rangle_t) - (1-\gamma) \cdot \frac{\partial}{\partial x}(\langle \rho \rangle \tilde{U} \langle u'u' \rangle_{\mathrm{st}} + \langle \rho \rangle \langle u'h' \rangle_{\mathrm{st}}) - (1-\gamma) \cdot \frac{\partial}{\partial y}(\langle \rho \rangle \tilde{U} \langle u'v' \rangle_{\mathrm{st}} + \langle \rho \rangle \langle v'h' \rangle_{\mathrm{st}}) \tag{2c}$$

In the previous equations, the subscripts st and t, respectively, refer to streaks and developed turbulence perturbations.

Table 1 Scaling parameters in the laminar zone (Prandtl scales)

Variable	Scaling value
$\tilde{U}$, u'	U_∞
$\tilde{V}$, $v' - \tilde{W}$, w'	$U_\infty/\sqrt{Re_L}$
ρ	ρ_∞
$\tilde{T}$, θ'	T_∞
$\tilde{P}$, π'	$\rho_\infty U_\infty^2/Re_L$

It is important to distinguish the two mechanisms implicitly included in these equations:

In the laminar zone, where the intermittency factor γ is equal to zero, the terms multiplied by $(1-\gamma)$ describes the transient-growth phenomenon: i.e., the Klebanoff-mode amplification.

The other terms, multiplied by γ, traditionally appear when considering turbulent equations. They numerically interfere when γ stops to be zero, i.e., when the turbulent spots appear, and within the fully turbulent region when γ tends toward one. In this study, the relationship for the intermittency function has been used by Arnal [17].

In the transition region, the two previous mechanisms coexist.

In the fully turbulent region, the apparent turbulent stresses $\langle u'v'\rangle_t$ and heat transfer $\langle u'h'\rangle_t$ are computed with a classical mixing-length model proposed by Michel et al. [21], which involves a turbulent viscosity μ_t given by relationship (3) and a turbulent conductivity λ_t given by Eq. (4) related to μ_t by a turbulent Prandtl number defined as a constant $P_t = 0.89$:

$$-\rho\langle u'v'\rangle_t = \mu_t\frac{\partial U}{\partial y} = -\rho F^2 l^2\left(\frac{\partial U}{\partial y}\right)^2$$

$$l/\delta = 0.085\tanh\left(\frac{\chi}{0.085}\frac{y}{\delta}\right), \qquad \chi = 0.41$$

$$F = 1-\exp\left(-\frac{l}{26\chi\mu}(\rho\tau)^{(1/2)}\right), \qquad \tau = \frac{\partial U}{\partial y} - \rho\langle u'v'\rangle_t \tag{3}$$

where l is the mixing length and F is the viscous-wall correction function.

The turbulent heat transfer is

$$-\rho\langle v'h'\rangle_t = \lambda_t\cdot\frac{\partial T}{\partial y} \tag{4}$$

The turbulent conductivity is

$$\lambda_t = \frac{\mu_t\cdot C_p}{P_t} \tag{5}$$

B. Klebanoff-Mode Equations

Perturbations equations are obtained employing the same scales (Table 1) as for the basic flow equations. Introducing the density weighted average (1) in the boundary-layer equations and keeping the first-order terms, two additional equations concerning streamwise velocity and temperature fluctuations are obtained:

$$\langle\rho\rangle\left(\frac{\partial u'}{\partial t}+\tilde{U}\frac{\partial u'}{\partial x}+\tilde{V}\frac{\partial u'}{\partial y}+u'\frac{\partial\tilde{U}}{\partial x}+v'\frac{\partial\tilde{U}}{\partial y}\right) = \frac{\partial}{\partial y}\left(\langle\mu\rangle\frac{\partial u'}{\partial y}\right)+\frac{\partial}{\partial z}\left(\langle\mu\rangle\frac{\partial u'}{\partial z}\right) \tag{6a}$$

$$\langle\rho\rangle C_p\left(\frac{\partial\theta'}{\partial t}+\tilde{U}\frac{\partial\theta'}{\partial x}+\tilde{V}\frac{\partial\theta'}{\partial y}+u'\frac{\partial\tilde{T}}{\partial x}+v'\frac{\partial\tilde{T}}{\partial y}\right) - \frac{\langle\rho\rangle C_p}{\tilde{T}}\theta'\left(\tilde{U}\frac{\partial\tilde{T}}{\partial x}+\tilde{V}\frac{\partial\tilde{T}}{\partial y}\right) = u'\frac{\partial\tilde{P}}{\partial x}+\mu'\theta'\left(\frac{\partial\tilde{U}}{\partial y}\right)^2 + 2\langle\mu\rangle\frac{\partial\tilde{u}'}{\partial y}\frac{\partial\tilde{U}}{\partial y}+\frac{\partial}{\partial y}\left(\langle\kappa\rangle\frac{\partial\theta'}{\partial y}\right)+\frac{\partial}{\partial z}\left(\langle\kappa\rangle\frac{\partial\theta'}{\partial z}\right)+\frac{\partial}{\partial y}\left(\kappa'\theta'\frac{\partial\tilde{T}}{\partial y}\right)$$

$$\text{With}\begin{pmatrix}\mu\\ \kappa\end{pmatrix} = \begin{pmatrix}\langle\mu\rangle\\ \langle\kappa\rangle\end{pmatrix}+\frac{\partial}{\partial T}\begin{pmatrix}\mu\\ \kappa\end{pmatrix}\cdot\theta' = \begin{pmatrix}\langle\mu\rangle\\ \langle\kappa\rangle\end{pmatrix}+\begin{pmatrix}\mu'\\ \kappa'\end{pmatrix}\cdot\theta' \tag{6b}$$

The perturbations are expressed in Fourier-transformed form, both in time and in spanwise direction according to the relation (7). The scalar product (subscript st) between two fluctuations a' and b' is reduced to the product of their amplitude [Eq. (8)]. Moreover, let us recall that optimal disturbance theory [11–14] has shown that the most amplified streaks were stationary (i.e., the frequency is zero: $\omega = 0$) and presented a well-defined spanwise wave number $\beta = 0.45$ for the incompressible boundary layer. These values ($\omega = 0$ and $\beta = 0.45$) will be used for the current modeling:

$$\begin{pmatrix}u'\\ \theta'\end{pmatrix} = \sum_{m,n}^{\infty}\begin{pmatrix}\tilde{u}'\\ \tilde{\theta}'\end{pmatrix}(x,y)\cdot\exp(i\beta_m z - i\omega_n t) \tag{7}$$

$$\langle a'b'\rangle_{\text{st}} = \frac{\omega}{2\pi}\frac{\beta}{2\pi}\int_t\int_z\tilde{a}'(x,y)e^{i(\beta z-\omega t)}\cdot\text{cc}[\tilde{b}'(x,y)e^{i(\beta z-\omega t)}] = \tilde{a}'(x,y)\tilde{b}'(x,y) \tag{8}$$

C. Closure of the System

At this stage, we have to solve three equations, Eqs. (2a–2c) for the mean flow completed by two additional transport equations, Eq. (6a) for the streamwise velocity fluctuation, and Eq. (6b) for the temperature fluctuation. The unknowns are the mean quantities ($\tilde{U}$, $\tilde{V}$, and $\tilde{T}$) and their fluctuating parts (u', v', and θ'). The density $\langle\rho\rangle$ and the mean temperature $\tilde{T}$ are linked by the equation of state ($\langle\rho\rangle\cdot\tilde{T} = \tilde{P}$). In the same way, the dynamic viscosity μ is obtained using the Sutherland law, and the conductivity is deduced using a constant Prandtl number such as $Pr = \langle\mu\rangle\times C_p/\langle\kappa\rangle$.

To close the system in the laminar region, the wall-normal velocity fluctuation has to be modeled. The model is intended to express the lift-up effect in accordance with the fact that a wall-normal velocity perturbation in a shear flow brings about emergence and amplification of streamwise velocity fluctuations (and temperature fluctuations for compressible flows [13]).

Using the boundary-layer scales of Table 1, all the dimensionless equations are parabolic. So if the wall-normal velocity is modeled, the system can be solved by a marching downstream procedure. The first step consists of solving the equations for the mean flow, taking into account the terms that describe the influence of the streaks; the values used to compute the coupling terms correspond to the value of the upstream station. The transport equations for u' and θ' are then solved. More details about the discretization and the resolution of the equations are described in Appendix A.

D. Bypass-Transition Criterion

The computation of the bypass-transition location is based on a classical approach that consists of comparing a quantity resulting from the calculation of the laminar boundary layer to a threshold value. Biau et al. [22] proposed the following expression:

$$\max_{\forall y}\left|(-\rho\cdot\langle u'v'\rangle_{\text{st}})\Big/\left(\mu\frac{\partial U}{\partial y}\right)\right| = C \tag{9}$$

From a physical point of view, this relationship expresses the fact that transition occurs only when the ratio between the driving term of streak formation ($\langle u'v'\rangle_{\text{st}}$) and the dissipative term ($\partial U/\partial y$) reaches a certain value.

III. Wall-Normal Velocity Fluctuation Modeling

A. Normalized Shape of the Wall-Normal Velocity Inside the Boundary Layer

The key stage now is to model the wall-normal velocity disturbances in order to close the previous system formed by Eqs. (2) and (6). Recent experimental data from Fransson and Westin [23] and Inasawa et al. [24] and DNS from Jacobs and Durbin [25] exhibit a monotonic profile for v'; moreover, at the boundary-layer outer edge, v' does not match with external freestream turbulence, but reaches only a fraction of it. A possible explanation for latter characteristic is that the normal velocity starts to be damped from a distance

comparable to external turbulence eddies and is not controlled by the boundary-layer thickness.

From these considerations, Biau et al. [22,26] proposed the function $G(y)$ [Eq. (10)] in order to represent the normalized wall-normal velocity fluctuation. This function ensures the no-slip condition and the respect of the continuity equation for the perturbation at the wall location. In addition, the parameter α is chosen in order to provide the continuity of the function at the edge of the boundary layer:

$$G(y) = \begin{cases} \frac{y^2 e^{-\alpha y}}{\max_y(y^2 e^{-\alpha y})} & \text{if } y \le \delta_{99} \\ 1 & \text{if } y > \delta_{99} \end{cases} \Rightarrow \begin{cases} \tilde{v}'(y=0) = 0 \\ \left(\frac{\partial \tilde{v}'}{\partial y}\right)_{y=0} = 0 \end{cases} \tag{10}$$

where

$$\alpha = \frac{2}{\delta_{99}} \quad \text{such as} \quad \left(\frac{\partial \tilde{v}'}{\partial y}\right)_{y=\delta_{99}} = 0$$

A normalized profile of the wall-normal velocity fluctuation is plotted and compared to the optimal disturbance theory [27] and the DNS results in Figure 1a. Note that outside the boundary layer, the values of v' do not match. Nonetheless, these different behaviors do not affect numerical results. As a matter of fact, the numerical simulations are intended to determine the amplification of Klebanoff modes, which are a direct outcome from the shear; outside the boundary layer, streaks are no longer generated, because $\mathrm{d}U/\mathrm{d}y = 0$. The corresponding Reynolds stress $\langle u'v' \rangle$ obtained using the v' model shows good agreement with the experimental data of Inasawa et al. [24] (Fig. 1b).

B. Streamwise Evolution of the Wall-Normal Velocity Fluctuation

A crucial point to study consists of the continuous forcing of the boundary layer by the external structure all along the outer edge of the boundary layer. To analyze this effect, boundary-layer responses to freestream turbulence and to isolated disturbance have to be compared. In 1985, Grek et al. [28], using a moderated-amplitude jet through a hole, applied an isolated and leading-edge localized disturbance to the boundary layer. Inside the boundary layer, they obtained a puff structure characterized by a narrow spanwise scale and a decaying amplitude. This puff structure was then identified as a subsiding high-speed streak surrounded by two low-speed streaks [29,30]. Alfredsson and Matsubara [31] also found decaying Klebanoff modes inside a boundary layer subjected to isolated disturbance, whereas they measured longitudinal amplified streaks when the boundary layer was subjected to a FST. Alfredsson and Matsubara concluded that the downstream development of the streaks depends, to a large extent, on the continuous forcing provided by the freestream turbulence all along the boundary-layer edge and is not restricted to the vicinity of the leading edge. In our modeling, the external forcing of the freestream turbulence on the boundary-layer streaks is taken into account by assuming that at the edge of the boundary layer, v' amplitude is directly proportional to the local freestream velocity disturbance $U_e(x) \times Tu_e(x) = u'_{e,\mathrm{rms}}(x)$. This assumption leads to the formulation (11) for the normal velocity fluctuation:

$$v'(x, y) = A_{\mathrm{st}} \times G(y) \times (U_e(x) \times Tu_e(x)) \tag{11}$$

In the previous model [22], the amplitude of v' depended on the value of the FST level at the leading edge Tu_0 and was therefore x-independent. This means that the previous model was not sensitive to the streamwise development of the freestream turbulence above the boundary layer. In particular, for the Jonàš et al. [15] experiments, for which $Tu_0 = 3\%$ in all cases, the previous model would have computed the same numerical streak amplification and thus the same bypass-transition location for whatever configurations. Nonetheless, the measurements have shown that for the same value of Tu_0, transition location was deeply influenced by the dissipative length scale of the external turbulence. With the current model, assuming that v' is directly proportional to the local freestream turbulence level Tu_e, we intend to capture such a mechanism. As a matter of fact, the FST level decrease all along the boundary-layer edge is defined by the dissipative length scale.

IV. Results

A. Calibration on Case T3A

The parameters A_{st} in Eq. (11) and C in Eq. (9) have to be determined. The calibration has been performed on the T3A case of Roach and Brierley's experiments [32]: mean flow quantities and fluctuations have been measured by a hot-wire technique inside a boundary layer developing on a flat plate subjected to grid turbulence, such as at the leading edge $Tu_0 = 3\%$, with an external constant velocity $U_e = 5.3$ m/s. The constant A_{st} has been fixed in such a way that the numerical streak amplitude, given by Eq. (12), matches the measurements (Fig. 2). The streak amplitude is defined as

$$\mathrm{amp}\,(x) = \max_{\forall y} |\tilde{u}'_{\mathrm{st}}(x, y)| \tag{12}$$

Figure 3 clearly shows that streak propagation inside the laminar zone alters the mean flow quantities. In the presence of Klebanoff modes, the streamwise velocity increases in the near-wall region but, in counterpart, decreases in the neighborhood of the boundary-layer edge. Therefore, streaks induce a momentum-thickness increase (Fig. 3b), while the displacement thickness remains quasi-constant. This leads to a decrease of the shape factor (Fig. 3c) even within the laminar zone, which is a typical distinguishing feature of streaky flows. The evolutions of the shape factor, of the Reynolds number momentum thickness, and of the skin-friction coefficient have been

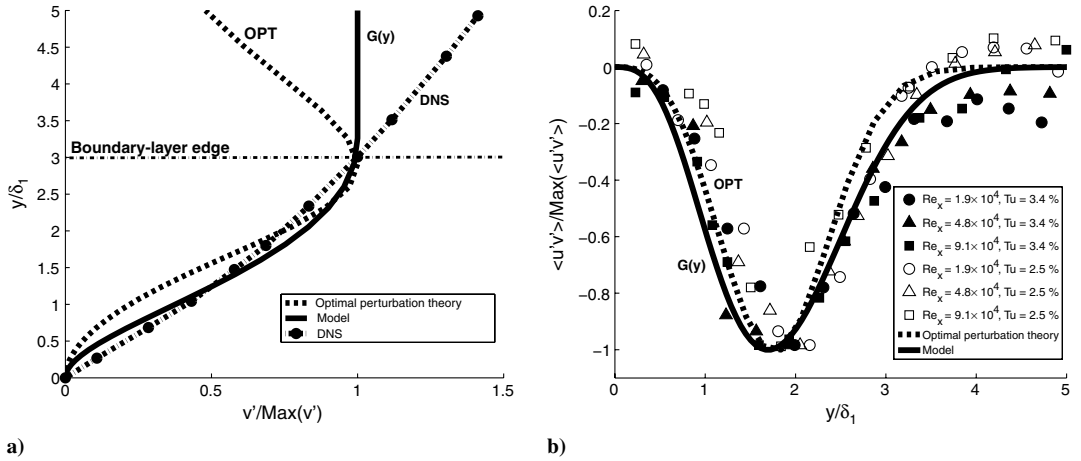

a) b)

Fig. 1 Plots of a) wall-normal velocity fluctuation v' with profiles normalized to unity at $y \approx 3 \cdot \delta_1$ and b) profile for the correlation $\overline{u'v'}$; OPT is the optimal perturbation theory [27], function $G(y)$ is from [22], DNS is from Jacobs and Durbin [25], and symbols on the right represent Inasawa et al.'s [24] experimental results for several longitudinal stations and two freestream turbulence levels.

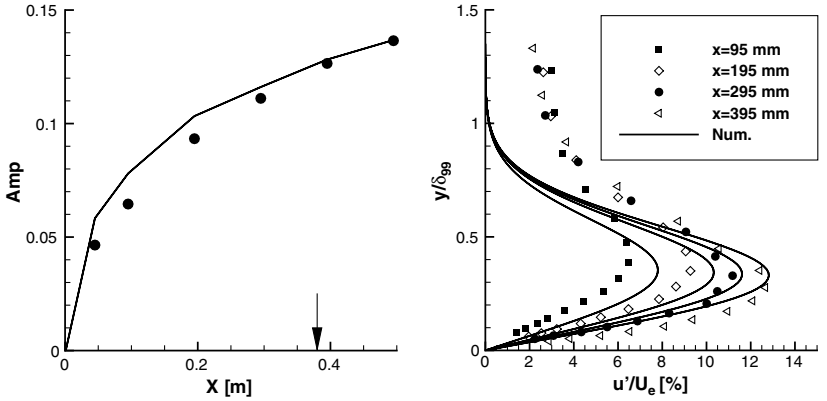

a) Streaks amplitude b) Streaks profiles

Fig. 2 Comparison between measurements and numerical simulations for the Klebanoff-mode case T3A. The arrow indicates the experimental transition location.

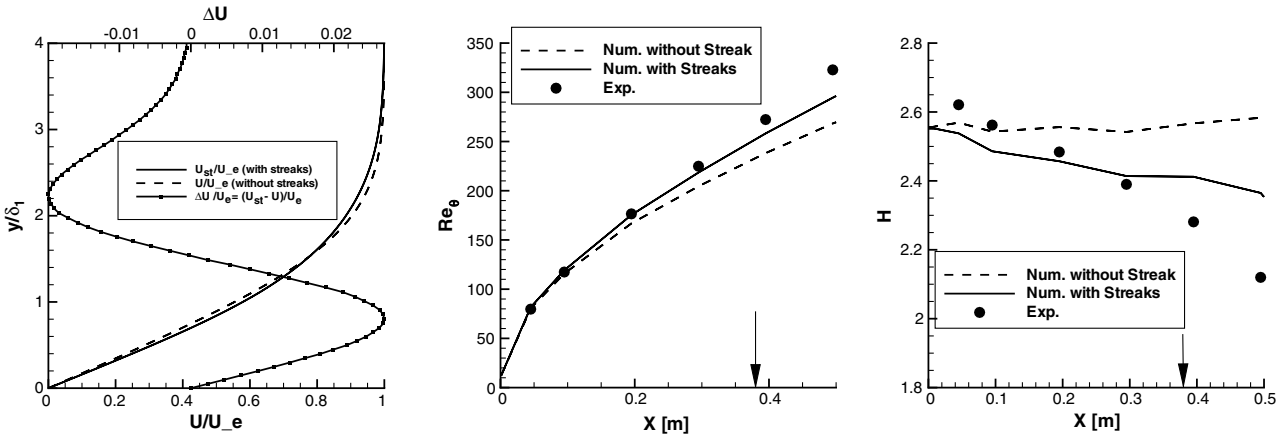

a) Streaks influence on the mean streamwise velocity profile b) Reynolds number based on the momentum thickness Re_θ c) Shape factor H

Fig. 3 Influence of the Klebanoff modes on the mean flow in the laminar region, case T3A. Arrows indicate the experimental transition location.

plotted in Fig. 4 throughout the whole plate: i.e., for the laminar, the transitional, and the fully turbulent regions. The vertical arrow represents the experimental transition location in that case: $x=$ 0.38 m. Assuming $C = 0.65$ gives a numerical transition onset at $x_{\text{num}} = 0.42$ m for the T3A case.

B. Influence of the External Flow Properties

The model has then been applied to different experimental data in order to investigate the influence of the external flow properties on the amplification of the Klebanoff modes and therefore on the bypass-transition location.

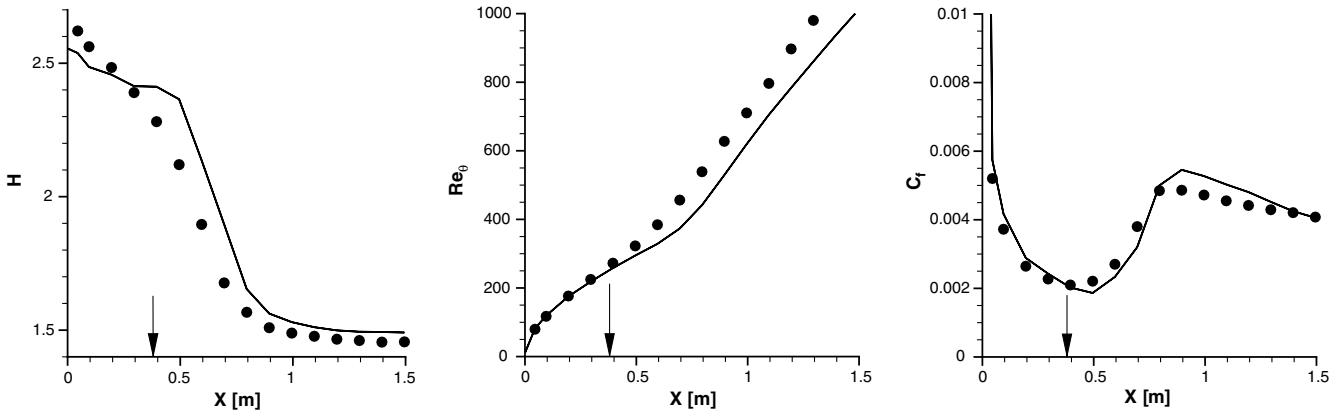

a) Shape factor H b) Reynolds number based on the momentum thickness Re_θ c) Skin friction coefficient

Fig. 4 Evolution of the boundary-layer parameters for the T3A case. Symbols are measurements, lines are numerical results, and arrows are experimental transition location.

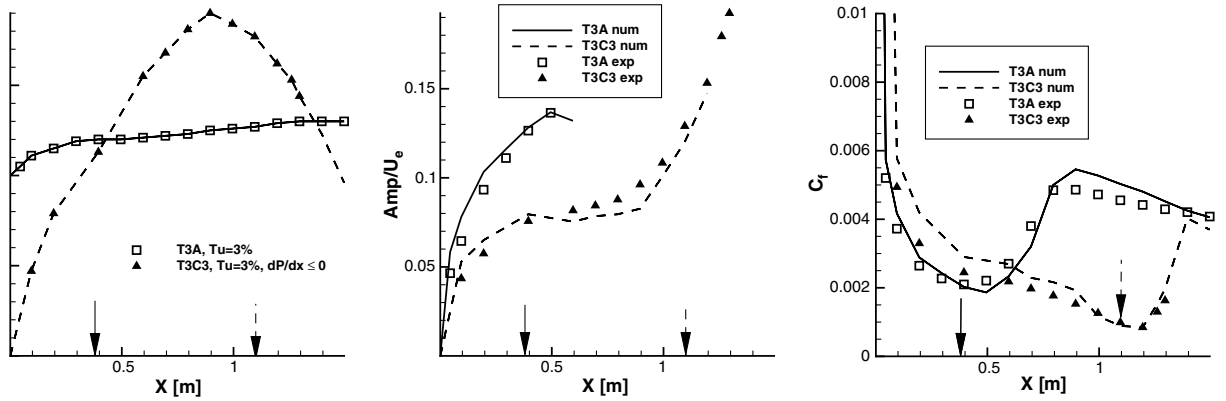

a) Evolution of the external velocity b) Streak Amplitude in the laminar zone c) Skin friction coefficient C_f

Fig. 5 Influence of the pressure gradient on the bypass-transition location. Comparison between the T3A and T3C3 cases. The arrows represent the corresponding experimental transition location for each case.

1. External Pressure Gradient

The first point studied here is the influence of the external pressure gradient on the stability of the Klebanoff modes. The model has first been applied to the T3C3 case, which is characterized by an initial accelerated flow followed by a deceleration (Fig. 5a). The freestream turbulence level at the leading edge is the same as in the T3A case: $Tu_0 = 3\%$. Figure 5b clearly shows that a favorable pressure gradient has a strong stabilizing effect. Thus, at $x = 0.4$ m, which corresponds to the T3A transition location, the amplitude of the streaks is only 7% of the external velocity, whereas it reaches 13% for the zero-pressure-gradient T3A case. In addition, we can see that as soon as the external flow starts to be decelerated, streak amplitude increases in a fast way, triggering the transition (as illustrated by the evolution of the skin-friction coefficient).

The same evolution has been measured at ONERA in a low-speed wind tunnel. The boundary layer was developing on a flat plate

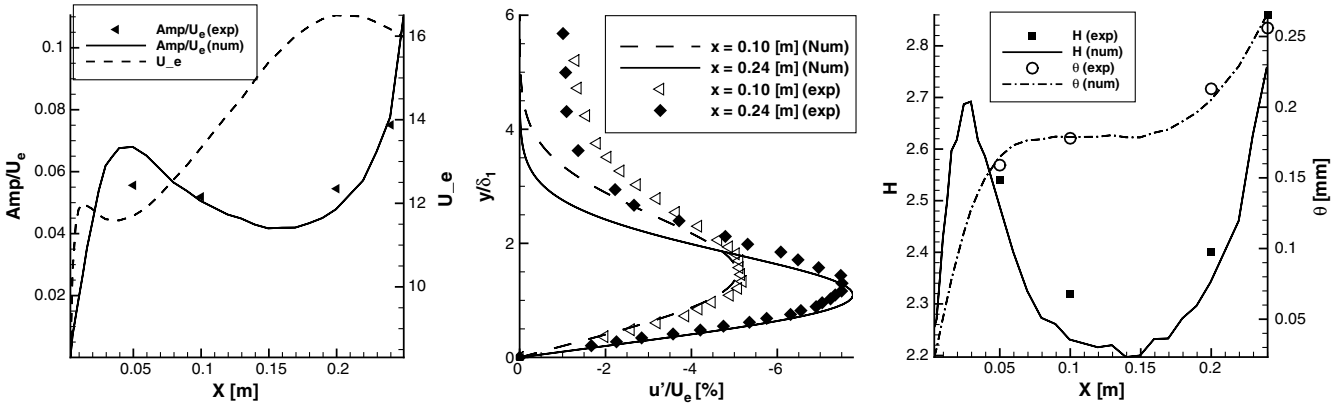

a) Streak amplitude evolution function of the external velocity b) Streak profiles c) Shape factor H and thickness momentum θ

Fig. 6 ONERA experiments.

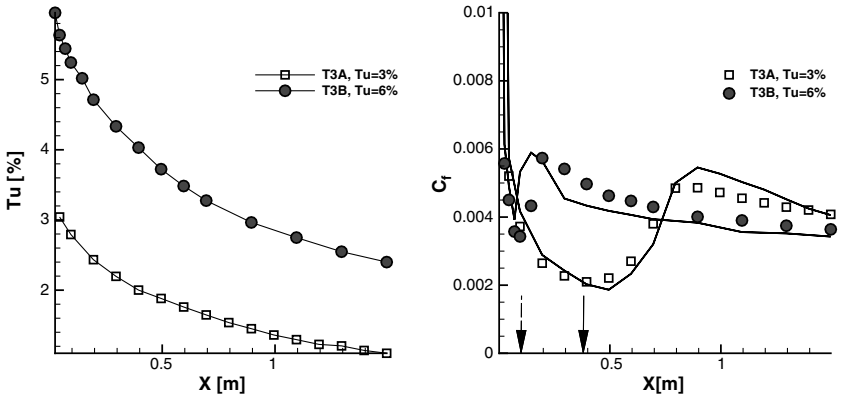

a) Evolution of the external free stream turbulence level Tu_e b) Skin friction coefficient C_f

Fig. 7 Influence of the freestream turbulence level on the bypass-transition location. Symbols are Roach and Brierley's [32] measurements, lines are numerical results, and arrows are experimental transition locations.

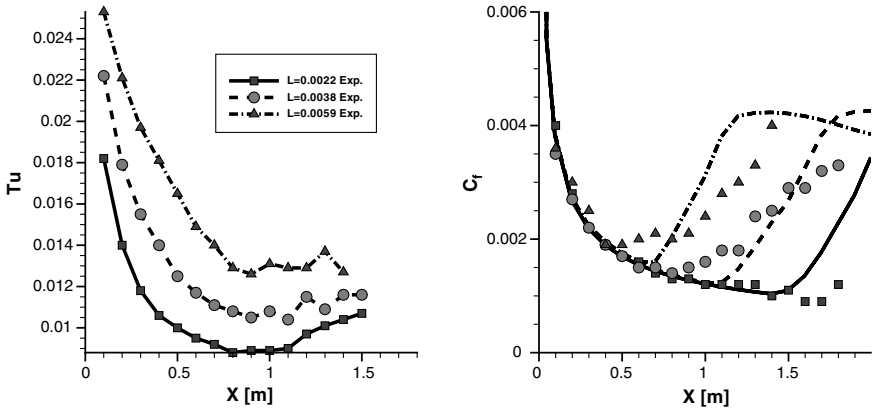

a) Evolution of the free stream turbulence level Tu_e for different dissipation length scale

b) Skin friction coefficient C_f function of the dissipative length scale

Fig. 8 Influence of the dissipation length scale of the bypass-transition location. Symbols correspond to Jonàš et al.'s [15] measurements.

placed into a typical turbine pressure gradient generated by a specific shape. The experimental results presented here concern hot-wire investigation of a boundary layer subjected to an external grid turbulence such that $Tu_0 = 2.2\%$ at the leading edge. Figure 6a illustrates the influence of the external velocity on the streaks. Between $x = 0.05$ and 0.15 m, where the acceleration is the strongest, the numerical amplitude of the streaks decreases. Furthermore, it is noticeable that even though our model has been calibrated on a zero-pressure-gradient case, it provides very good results for both the amplitude of the streaks and for the corresponding fluctuation profiles (Fig. 6b). There is a restriction for the first measurement point ($x = 0.05$ m), where the numerical amplitude is overestimated. The shape factor and the corresponding momentum thickness have been reported in Fig. 6c. In these experiments, transition occurs in a separation bubble starting at $x = 0.25$ m and thus cannot be predicted by the boundary-layer approach used in this study.

2. *Influence of the Freestream Turbulence*

The T3B case is characterized by high-amplitude freestream disturbances, such as $Tu = 6\%$ at the leading edge of the flat plate. The streamwise evolution of the corresponding freestream turbulence level is plotted in Fig. 7a and compared with our reference case (T3A). The respective skin-friction coefficients are presented in Fig. 7b; when Tu increases, the Klebanoff modes developing within the laminar boundary layer gain more energy, and so bypass transition occurs earlier. For the T3B case, the laminar region is localized in the leading-edge region, and transition happens for $x = 0.1$ m.

Moreover, Jonàš et al.'s experimental data [15] have highlighted the fact that Klebanoff-mode propagation depended not only on the level, but also on the scales, of the freestream turbulence. The dissipative length scale is defined as in Hancock and Bradshaw [33] by

$$L_e = -(\langle u'^2\rangle)_e^{3/2} \Big/ \left(\tilde{U}_e \cdot \frac{\mathrm{d}(\langle u'^2\rangle)_e}{\mathrm{d}x}\right) \tag{13}$$

Turbulent flow with a large length scale has a smaller dissipation rate, and thus decays less rapidly in the flow direction (see Fig. 8a). Therefore, for different dissipative length scales, the boundary layer is not disturbed in the same manner. The upstream conditions in Jonàš et al.'s experiments [15] are the same as those of the T3A case: a freestream turbulence level $Tu_0 = 3\%$ at the leading edge for a freestream velocity $U_0 = 5$ m/s. In the present model, the amplitude of the wall-normal velocity fluctuation is proportional to the local freestream turbulence level $v' \propto Tu_e(x)$; the onset of numerical bypass transition moves upstream for increasing dissipative length scale in accordance with the measurements. For the two most important dissipative length scales, the model provides later numerical transition position than that of the experiment. In addition, the numerical increase of the skin-friction coefficient in the transitional region is too abrupt. The numerical slope of the C_f is driven by the intermittency function [17], which has been calibrated on experiments with positive or zero-pressure-gradient flows. Under the present circumstances, no satisfying reasons can explain the discrepancy, especially since the intermittency function provides good results for the Roach and Brierley [32] measurements (in particular, for the T3A case, which has the same FST level at the leading edge as all the cases of Jonàš et al. [15]). The present model has not been applied to compressible flows, because we did not find any experiments in the published literature showing the amplification of Klebanoff modes induced by FST inside compressible boundary layers. As a matter of fact, for wind-tunnel experiments, when the Mach number increases, the noise (i.e., pressure fluctuations) radiated by the wall of the wind tunnel strongly increases and overwhelms the velocity fluctuations. Spectral analyses seem to demonstrate that in this configuration, the transition is driven by the TS wave amplification; the external pressure fluctuations increase the initial amplitude of the TS waves, as suggested by Mack [34].

3. *Bypass-Position Location*

The present simulation has been applied to several cases of Roach and Brierley [32] experiments in order to compare the numerical transition location with the measured location. The first two cases (T3A and T3B) concern zero-pressure-gradient flows with respective inlet turbulence levels of $Tu_0 = 3$ and 6%. The five other cases are characterized by a favorable negative pressure gradient in the first part of the plate. These cases are intended to roughly simulate flow over turbomachinery blades. The T3C1 case is highly perturbed with $Tu_0 = 6.6\%$. For the other cases $Tu_0 = 3\%$, and the inlet velocity is

Table 2 Comparison between experimental data and numerical results

				x_T	
Case	U_∞, m/s	$\mathrm{d}P/\mathrm{d}x$	Tu_0, %	Exp.	Num.
		Roach and Brierley [32]:			
T3A	5.4	0	3	0.38	0.42
T3B	9.4	0	6	0.10	0.07
T3C1	5.9	$\neq 0$	6.6	0.18	0.10
T3C2	5	$\neq 0$	3	0.80	0.7
T3C3	3.7	$\neq 0$	3	1.10	1.1
T3C4	1.2	$\neq 0$	3	1.25	1.4
T3C5	8.4	$\neq 0$	3	0.32	0.22
		Jonàš et al. [15]			
$L_e = 2.2$ mm	5	0	3	1.6	1.41
$L_e = 3.8$ mm	5	0	3	0.8	1.01
$L_e = 5.9$ mm	5	0	3	0.5	0.62

Table 3 Criterion sensitivity comparison between measurements and numerical results

Case	Exp	$C = 0.585$ (−10%)	$C = 0.65$ (ref. value)	$C = 0.715$ (+10%)
		Roach and Brierley [32]:		
T3A	0.38	0.35	0.42	0.52
T3B	0.10	0.06	0.07	0.08
T3C1	0.18	0.09	0.10	0.11
T3C2	0.80	0.52	0.70	0.89
T3C3	1.10	0.91	1.10	——
T3C4	1.25	1.40	1.40	1.40
T3C5	0.32	0.19	0.22	0.25
		Jonàš et al. [15]:		
$L_e = 2.2$ mm	1.6	1.38	1.41	1.44
$L_e = 3.8$ mm	0.8	0.89	1.02	1.14
$L_e = 5.9$ mm	0.5	0.41	0.62	0.80

gradually reduced to delay the abscissa of transition. Results are summarized in Table 2.

4. *Criterion Sensitivity*

The bypass criterion sensitivity has been analyzed by varying the value of the transition threshold C by 10% around the calibrated value $C = 0.65$. The modified transition location has been computed for each case and is summarized in Table 3. It is clear that the position of the transition is sensitive to the threshold value. As a matter of fact, a difference of 10% in the value of C will induce a 25% variation in the numerical transition location. The evolution of the quantity $\langle u'v'\rangle/(\nu\partial U/\partial y)$ has been plotted in Fig. 9a. The variance on the numerical transition location becomes more important when the slope of the criterion decreases. The evolution of the skin-friction coefficient for the T3A case of the Roach and Brierley experiment [32] computed with three values of the threshold ($C = 0.585$, 0.65, and 0.715) is plotted in Fig. 9b and compared to the experimental data.

V. Conclusions

A simplified model based on the resolution of two transport equations and intended to predict the bypass-transition location has been presented. This model is an improvement of the previous one proposed by Biau et al. [22]; it has been introduced in a boundary-layer code, which allows computing the whole bypass-transition process from the amplification of the Klebanoff modes in the laminar part to the fully turbulent region. Moreover, the dependency of the modeled wall-normal velocity fluctuation on local freestream turbulence level has been introduced in order to take into account the spatial evolution of the external turbulence above the boundary-layer edge. The model is not focused on describing all the physical mechanisms that trigger transition; in particular, the linearity of the two transport equations does not allow capture of the secondary inflectional instability that leads to the breakdown into turbulent spots. Nevertheless, the dynamics of Klebanoff modes within the laminar zone have been numerically determined and used to estimate the transition location. The present model gives coherent results for boundary layers subjected to high external turbulence levels, in agreement with experimental data. The model has been theoretically developed for compressible boundary layers, but for the time being, it has just been tested in the limit of incompressible boundary layers, for which several experimental data exist. The logical following task is to extend this study to supersonic flows for which transient growth still exists. In the same way, the same modeling technique will be applied to study roughness-induced transition. In particular, transient growth is a plausible explanation for the blunt-body paradox [35], which refers to the early transition on forebody at supersonic flows in a region where TS waves are stabilized. Indeed, Fransson et al. [36] measured transient growth behind an array of roughness elements. Future effort will concentrate on the v' formulation, which may be different from the formulation representing the effect of freestream turbulence.

Appendix A: Discretization of the Equations

In this Appendix, we describe the discretization and the resolution of the longitudinal mean velocity equaiton (A1):

$$\langle\rho\rangle\tilde{U}\frac{\partial\tilde{U}}{\partial x} + \langle\rho\rangle\tilde{V}\frac{\partial\tilde{U}}{\partial y} = \rho_e U_e\frac{\mathrm{d}U_e}{\mathrm{d}x} + \frac{\partial}{\partial y}\left(\langle\mu\rangle\frac{\partial\tilde{U}}{\partial y}\right) - \gamma\cdot\overbrace{\frac{\partial\langle\rho\rangle\langle u'v'\rangle_t}{\partial y}}^{-\mu_t\cdot(\partial U/\partial y)} - (1-\gamma)\cdot\left(-\frac{\partial\langle\rho\rangle\langle u'u'\rangle_{\mathrm{st}}}{\partial x} - \frac{\partial\langle\rho\rangle\langle u'v'\rangle_{\mathrm{st}}}{\partial y}\right) \tag{A1}$$

Introducing the expression of the turbulent viscosity, the previous equation is reduced to

$$\langle\rho\rangle\tilde{U}\frac{\partial\tilde{U}}{\partial x} + \langle\rho\rangle\tilde{V}\frac{\partial\tilde{U}}{\partial y} = \rho_e U_e\frac{\mathrm{d}U_e}{\mathrm{d}x} + \frac{\partial}{\partial y}\left(\underbrace{(\langle\mu\rangle + \gamma\cdot\mu_t)}_{\mu_{\mathrm{eff}}}\frac{\partial\tilde{U}}{\partial y}\right) - (1-\gamma)\cdot\left(-\frac{\partial\langle\rho\rangle\langle u'u'\rangle_{\mathrm{st}}}{\partial x} - \frac{\partial\langle\rho\rangle\langle u'v'\rangle_{\mathrm{st}}}{\partial y}\right) \tag{A2}$$

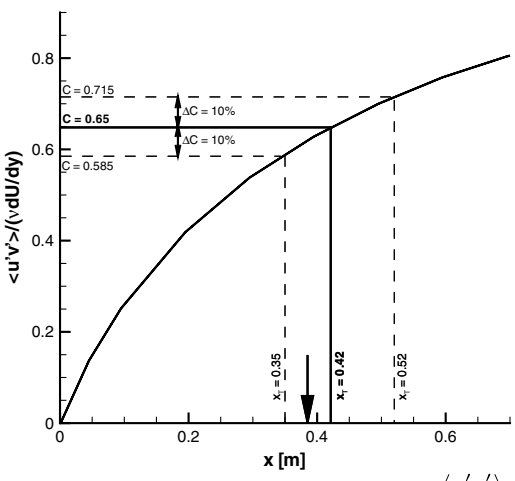

a) Evolution of the by pass transition criterion $\frac{\langle u'v'\rangle}{\nu\partial U/\partial y}$

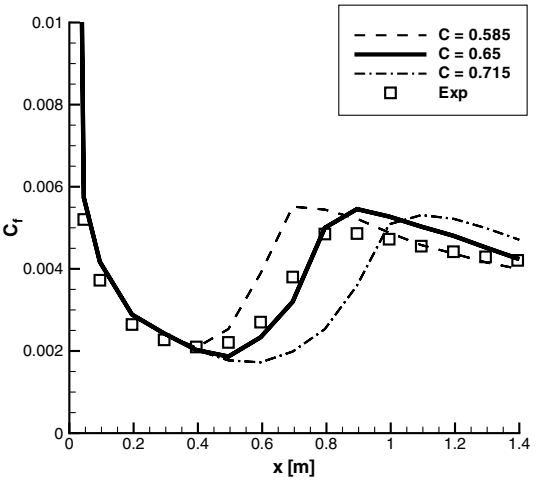

b) Skin friction coefficient C_f function of the value of the transition threshold C

Fig. 9 Influence of the criterion threshold on the transition location and the evolution of the skin friction for the T3A case. Symbols correspond to Roach and Brierley's [32] measurements, and the arrow indicates the experimental transition location.

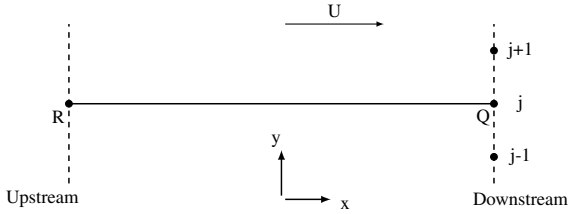

Fig. A1 Discretization scheme.

The longitudinal mean velocity equation is then discretized according to the notations of the scheme of Fig. A1. In particular, the diffusive term is treated on three consecutive points between y_{j-1} and y_j:

$$\langle\rho\rangle_j^R \tilde{U}_j^R \frac{\tilde{U}_j^Q - \tilde{U}_j^R}{x_j^Q - x_j^R} + \langle\rho\rangle_j^R \tilde{V}_j^R \frac{\tilde{U}_{j+1}^Q - \tilde{U}_{j-1}^Q}{2\Delta_j} = \rho_e^R U_e^R \frac{U_e^Q - U_e^R}{x_j^Q - x_j^R}$$
$$+ (\mu_{\text{eff}})_{j+1/2}^R \frac{\tilde{U}_{j+1}^Q - \tilde{U}_j^Q}{2\Delta_j\Delta_{j+1/2}} - (\mu_{\text{eff}})_{j-1/2}^R \frac{\tilde{U}_j^Q - \tilde{U}_{j-1}^Q}{2\Delta_j\Delta_{j-1/2}} + (\gamma+1)$$
$$\cdot [(\langle\rho\rangle\langle u'u'\rangle_x)_j^R + (\langle\rho\rangle\langle u'v'\rangle_y)_j^R]$$
$$\text{With: } \Delta_j = \frac{y_{j+1} - y_{j-1}}{2}, \qquad \Delta_{j+1/2} = y_{j+1} - y_j$$
$$\mathrm{d}x_j = x_j^Q - x_j^R \quad \text{and} \quad (\mu_{\text{eff}})_{j+1/2} = \frac{\mu_{j+1} + \mu_j}{2} \tag{A3}$$

The previous equation can be written with the following matrix form:

$$a_j(\tilde{U})_{j-1}^Q + b_j(\tilde{U})_j^Q + c_j(\tilde{U})_{j+1}^Q = d_j \tag{A4}$$

where

$$a_j = -\frac{\langle\rho\rangle_j^R \tilde{V}_j^R}{\Delta_j} - \frac{(\mu_{\text{eff}})_{j-1/2}^R}{\Delta_j\Delta_{j-1/2}}$$
$$c_j = \frac{\langle\rho\rangle_j^R \tilde{V}_j^R}{\Delta_j} - \frac{(\mu_{\text{eff}})_{j+1/2}^R}{\Delta_j\Delta_{j+1/2}}$$
$$b_j = -(a_j + c_j) + \langle\rho\rangle_j^R \tilde{U}_j^R \frac{1}{\mathrm{d}x_j}$$
$$d_j = \langle\rho\rangle_j^R \tilde{U}_j^R \frac{\tilde{U}_j^R}{\mathrm{d}x_j} + \rho_J^R U_J^R \frac{U_J^Q - U_J^R}{\mathrm{d}x_J} \tag{A5}$$

where $\tilde{U}_J = \tilde{U}_e$ at the outer edge of the boundary layer and $\partial\tilde{U}/\partial y$ imposed at the wall. This problem will be solved using the tridiagonal matrix algorithm also known as the Thomas algorithm:

$$\begin{pmatrix} a_2 & b_2 & c_2 & \cdots & \cdots & 0 \\ 0 & a_3 & b_3 & c_3 & \cdots & 0 \\ 0 & \cdots & \ddots & \ddots & \ddots & c_{J-1} \\ 0 & \cdots & \cdots & \cdots & a_J & b_J \end{pmatrix} \times \begin{pmatrix} U_1^Q \\ U_2^Q \\ U_3^Q \\ \vdots \\ U_J^Q \end{pmatrix} = \begin{pmatrix} d_1 \\ d_2 \\ d_3 \\ \vdots \\ d_J \end{pmatrix} \tag{A6}$$

The first step, called the forward step, consists of modifying the coefficient as follows for j varying from 2 to J:

$$\alpha_j = \begin{cases} -\frac{c_1}{b_1} & \text{for } j = 1 \\ -\frac{c_j}{b_j + a_j\cdot\alpha_{j-1}} & \text{for } j = 2, \ldots, J \end{cases} \tag{A7}$$

$$\beta_j = \begin{cases} \frac{d_1}{b_1} & \text{for } j = 1 \\ \frac{d_j - a_j\cdot\beta_{j-1}}{b_j + a_j\cdot\alpha_{j-1}} & \text{for } j = 2, \ldots, J \end{cases} \tag{A8}$$

The solution is then obtained by backsubstitution from the outer edge of the boundary layer $j = J$ to the wall $j = 1$:

$$\tilde{U}_J = U_e, \qquad \tilde{U}_j = \alpha_j\tilde{U}_{j+1} + \beta_j \tag{A9}$$

where α_1 and β_1 depend on the wall boundary conditions. Concerning the longitudinal velocity, the no-slip condition $\tilde{U}_1 = 0$ imposed $\alpha_1 = \beta_1 = 0$. For the energy equation, the discretization and the resolution are exactly the same. If the wall temperature $T = T_w$ is imposed, this will lead to $\alpha_1 = 0$ and $\beta_1 = T_w$. If it is the wall heat transfer that is known, $(\partial T/\partial y)_w$, we will have $\alpha_1 = 1$ and $\beta_1 = -(y_2 - y_1) \times (\partial T/\partial y)_w$.

References

[1] Matsubara, M., and Alfredsson, P., "Disturbances Growth in Boundary Layers Subjected to Free-Stream Turbulence," *Journal of Fluid Mechanics*, Vol. 430, 2001, pp. 149–168. doi:10.1017/S0022112000002810

[2] Westin, K., Boiko, A., Klingmann, B., Kozlov, V., and Alfredsson, P., "Experiments in a Boundary Layer Subjected to Free Stream Turbulence. Part I. Boundary Layer Structure and Receptivity," *Journal of Fluid Mechanics*, Vol. 281, 1994, pp. 193–218. doi:10.1017/S0022112094003083

[3] Klebanoff, P., "Effect of Free-Stream Turbulence on a Laminar Boundary Layer," *Bulletin of the American Physical Society*, Vol. 16, 1971.

[4] Arnal, D., and Juillen, J., "Contribution Expérimentale à l'Étude de la Réceptivité d'une Couche Limite à la Turbulence de l'Écoulement Général," Vol. 1, ONERA, Rept. 5018 AYD, 1978.

[5] Kendall, J. M., "Experimental Study of Disturbances Produced in a Pretransitional Laminar Boundary Layer by Weak Freestream Turbulence," AIAA Paper 85-1695, 1985.

[6] Henningson, D., "Comment on 'Transition in Shear Flows. Nonlinear Normality Versus Non-Normal Linearity'," *Physics of Fluids*, Vol. 8, Aug. 1996, pp. 2257–2258. doi:10.1063/1.869011

[7] Schmid, P., and Henningson, D., *Stability and Transition in Shear Flows*, Vol. 142, Springer, New York, 2001.

[8] Trefethen, L., Trefethen, A., Reddy, S., and Driscoll, T., "Hydrodynamic Stability Without Eigenvalues," *Science*, Vol. 261, No. 5121, 1993, pp. 578–584. doi:10.1126/science.261.5121.578

[9] Ellingsen, T., and Palm, E., "Stability of Linear Flow," *Physics of Fluids*, Vol. 18, No. 4, 1975, p. 487. doi:10.1063/1.861156

[10] Landahl, M., "A Note on Algebraic Instability of Inviscid Parallel Shear Flows," *Journal of Fluid Mechanics*, Vol. 98, No. 2, 1980, pp. 243–251. doi:10.1017/S0022112080000122

[11] Andersson, P., Berggren, M., and Henningson, D., "Optimal Disturbances and Bypass Transition in Boundary Layers," *Physics of Fluids*, Vol. 11, No. 1, Jan. 1999, pp. 134–150. doi:10.1063/1.869908

[12] Luchini, P., "Reynolds-Number-Independent Instability of the Boundary Layer Over a Flat Surface: Optimal Perturbation," *Journal of Fluid Mechanics*, Vol. 404, 2000, pp. 289–309. doi:10.1017/S0022112099007259

[13] Tumin, A., and Reshotko, E., "Optimal Disturbances in Compressible Boundary Layers," *AIAA Journal*, Vol. 41, No. 12, Dec. 2003, pp. 2357–2363. doi:10.2514/2.6860

[14] Zuccher, S., Tumin, A., and Reshotko, E., "Parabolic Approach to Optimal Perturbations in Compressible Boundary Layers," *Journal of Fluid Mechanics*, Vol. 556, 2006, pp. 189–216. doi:10.1017/S0022112006009451

[15] Jonáš, P., Mazur, O., and Uruba, V., "On the Receptivity of the Bypass Transition to the Length Scale of the Outer Stream Turbulence," *European Journal of Mechanics, B/Fluids*, Vol. 19, 2000, pp. 707–722. doi:10.1016/S0997-7546(00)01094-3

[16] Brandt, L., Schlatter, P., and Henningson, D., "Transition in Boundary Layers Subject to Free-Stream Turbulence," *Journal of Fluid Mechanics*, Vol. 517, 2004, pp. 167–198. doi:10.1017/S0022112004000941

[17] Arnal, D., "Stabilité et Transition des Couches Limites Laminaires Bidimensionnelles en Écoulement Compressible sur Paroi Athermane," *La Recherche Aérospatiale*, Vol. 4, July–Aug. 1988, pp. 15–32.

[18] Jacobs, R., and Durbin, P., "Shear Sheltering and the Continuous Spectrum of the Orr-Sommerfeld Equation," *Physics of Fluids*, Vol. 10, 1998, pp. 2006–2011. doi:10.1063/1.869716

[19] Hernon, D., Walsh, E., and McEligot, D., "Experimental Investigation into the Routes to Bypass Transition and the Shear-Sheltering Phenomenon," *Journal of Fluid Mechanics*, Vol. 591, 2007, pp. 461–

479.
doi:10.1017/S0022112007008336
[20] Prandtl, L., "Ueber Flussigheitsbewegung bei sehr Kleiner Reibung," *Proceedings of the 3rd International Mathematical Congress*, Heidelberg, Germany, 1904.
[21] Michel, R., Quemard, C., and Durant, R., "Application d'un Schéma de Longueur de Mélange à l'Étude de Couches Limites d'Équilibre," ONERA Rept. 154, 1969.
[22] Biau, D., Arnal, D., and Vermeersch, O., "A Transition Prediction Model for Boundary Layers Subjected to Free-Stream Turbulence," *Aerospace Science and Technology*, Vol. 11, 2007, pp. 370–375.
doi:10.1016/j.ast.2006.08.011
[23] Fransson, J., and Westin, K., "Errors in Hot-Wire X-Probe Measurements Induced by Unsteady Velocity Gradients," *Experiments in Fluids*, Vol. 32, 2002, pp. 413–415.
doi:10.1007/s003480100360
[24] Inasawa, A., Lundell, F., Matsubara, M., Kohama, Y., and Alfredsson, P., "Velocity Statistics and Flow Structures Observed in Bypass Transition Using Stereo PTV," *Experiments in Fluids*, Vol. 34, 2003, pp. 242–252.
doi:10.1007/s00348-002-0551-3
[25] Jacobs, R., and Durbin, P., "Simulation of Bypass Transition," *Journal of Fluid Mechanics*, Vol. 428, 2001, pp. 185–212.
doi:10.1017/S0022112000002469
[26] Biau, D., "Etude des Structures Longitudinales dans la Couche Limite Laminaire et de leur lien avec la Transition," Ph.D. Thesis, École Nationale Supérieure de l'Aéronautique et de l'Espace, Toulouse, France, Oct. 2006.
[27] Vermeersch, O., "Théorie des Croissances Transitoires pour une Couche Limite Compressible," ONERA, Rept. RT 1/12668 DMAE, Oct. 2007.
[28] Grek, G., Kozlov, V., and Ramasanov, M., "Three Types Of Disturbances from the Point Source in the Boundary Layer," *Laminar-Turbulent Transition*, edited by V. V. Kozlov, Springer—Verlag, Berlin, Vol. 2, 1985, pp. 267–272.
[29] Bakchinov, A., Westin, K., Kozlov, V., and Alfredsson, P., "On the Receptivity of a Flat Plate Boundary Layer to Localized Free Stream Disturbances," *Laminar-Turbulent Transition*, edited by R. Kobayashi, Springer—Verlag, Berlin, 1995, pp. 341–348.
[30] Westin, K., Bakchinov, A., Kozlov, V., and Alfredsson, P., "Experiments on Localized Disturbances in a Flat Plate Boundary Layer. Part I: The Receptivity and Evolution of a Localized Free Stream Disturbance," *European Journal of Mechanics, B/Fluids*, Vol. 17, 1998, pp. 823–846.
doi:10.1016/S0997-7546(99)80016-8
[31] Alfredsson, P., and Matsubara, M., "Streaky Structures in Transition," *Transitional Boundary Layers in Aeronautics*, edited by R. A. W. M. Henkes, and J. L. van Ingen, North-Holland, Amsterdam, 1996, pp. 373–386.
[32] Roach, P., and Brierley, D., "The Influence of a Turbulent Free-Stream on Zero Pressure Gradient Transitional Boundary Layer Development. Part I. Test Cases T3A and T3B," *Numerical Simulation of Unsteady Flows and Transition to Turbulence*, Cambridge Univ. Press, New York, 1990.
[33] Hancock, P., and Bradshaw, P., "Turbulent Structure of a Boundary Layer Beneath a Turbulent Free Stream," *Journal of Fluid Mechanics*, Vol. 205, 1989, pp. 45–76.
doi:10.1017/S0022112089001941
[34] Mack, L., "Linear Stability Theory and the Problem of Supersonic Boundary Layer Transition," *AIAA Journal*, Vol. 13, No. 3, 1975, pp. 278–289.
doi:10.2514/3.49693
[35] Tumin, A., and Reshotko, E., "The Blunt Body Paradox—A Case For Transient Growth," *Laminar-Turbulent Transition*, edited by H. F. Fasel, and W. S. Saric, Springer–Verlag, Berlin, 1999, pp. 403–408.
[36] Fransson, J., Brandt, L., Talamelli, A., and Cossu, C., "Experimental Study of the Stabilization of Tollmien–Schlichting Waves by Finite Amplitude Streaks," *Physics of Fluids*, Vol. 17, No. 5, 2005, Paper 054110.
doi:10.1063/1.1897377

X. Zhong
Associate Editor